An anti-hapten camelid antibody reveals a cryptic binding site with significant energetic contributions from a nonhypervariable loop

Sean W. Fanning[1] and James R. Horn[1,2]*

[1]Department of Chemistry and Biochemistry, Northern Illinois University, DeKalb, IL 60115
[2]Center for Biochemical and Biophysical Studies, Northern Illinois University, DeKalb, IL 60115

Received 4 March 2011; Revised 26 April 2011; Accepted 26 April 2011
DOI: 10.1002/pro.648
Published online 6 May 2011 proteinscience.org

Abstract: Conventional anti-hapten antibodies typically bind low-molecular weight compounds (haptens) in the crevice between the variable heavy and light chains. Conversely, heavy chain-only camelid antibodies, which lack a light chain, must rely entirely on a single variable domain to recognize haptens. While several anti-hapten VHHs have been generated, little is known regarding the underlying structural and thermodynamic basis for hapten recognition. Here, an anti-methotrexate VHH (anti-MTX VHH) was generated using grafting methods whereby the three complementarity determining regions (CDRs) were inserted onto an existing VHH framework. Thermodynamic analysis of the anti-MTX VHH CDR1-3 Graft revealed a micromolar binding affinity, while the crystal structure of the complex revealed a somewhat surprising noncanonical binding site which involved MTX tunneling under the CDR1 loop. Due to the close proximity of MTX to CDR4, a nonhypervariable loop, the CDR4 loop sequence was subsequently introduced into the CDR1-3 graft, which resulted in a dramatic 1000-fold increase in the binding affinity. Crystal structure analysis of both the free and complex anti-MTX CDR1-4 graft revealed CDR4 plays a significant role in both intermolecular contacts and binding site conformation that appear to contribute toward high affinity binding. Additionally, the anti-MTX VHH possessed relatively high specificity for MTX over closely related compounds aminopterin and folate, demonstrating that VHH domains are capable of binding low-molecular weight ligands with high affinity and specificity, despite their reduced interface.

Keywords: camelid antibody; VHH, hapten; single domain antibody; VHH structure; CDR grafting; anti-hapten antibody; binding thermodynamics

Introduction

Antibodies play an important role in the immune response and serve as indispensible affinity reagents for numerous life science applications. They are well known for their ability to achieve high affinity and selectivity for their protein (i.e., antigen) and low-molecular weight molecule (i.e., hapten) targets. IgG antibodies that target haptens are particularly interesting, as they are not typically generated through a traditional immune response alone but require covalent conjugation to an immunogenic protein prior to animal immunization. Consequently, these anti-hapten antibodies provide unique insight into immune recognition. Additionally, anti-hapten antibodies can be used for numerous applications, such as assessing environmental and nutritional toxins,[1–3] separating enantiomeric compounds,[4] and

Abbreviations: AMT, aminopterin; CDR, complementarity determining regions; FOL, folate; MTX, methotrexate

Additional Supporting Information may be found in the online version of this article.

Grant sponsor: American Heart Association.

**Correspondence to:* James R. Horn, Department of Chemistry and Biochemistry, Northern Illinois University, DeKalb, IL 60115. E-mail: jrhorn@niu.edu

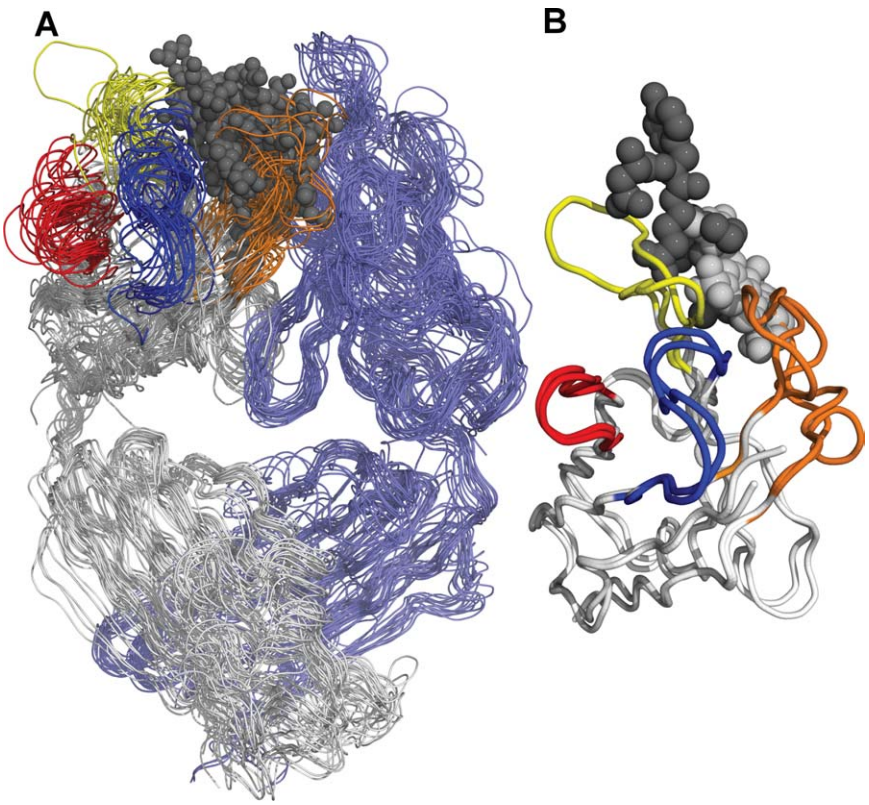

Figure 1. (A) Ribbon overlay of published hapten/anti-hapten antibody complexes. The nonredundant dataset includes 33 complexes (21 Fabs, 10 scFvs). Hapten atoms are presented as grey spheres. CDR1 (blue), CDR2 (yellow), CDR3 (orange), CDR4 (red). The overlay includes the following pdb files: 1QYG, 1BAF, 1C1E, 1C5C, 1CF8, 1F3D, 1FIG, 1FL6, 1IND, 1JNH, 1NGP, 1OAR, 1UM4, 1WCB, 1WZ1, 1X9Q, 1YOL, 2BMK, 2CGR, 2CJU, 2G2R, 2UUD, 3CFB, 3CFT, 3FO0, 1QD0, 1I3U, and 2X6M. (B) Overlay of an anti-RR1 VHH (RR1-light grey spheres) and anti-DYEPEA peptide VHH (peptide-dark grey spheres).

removing toxic medications[5,6] and illicit drugs from the body.[7]

The structural and energetic details of anti-hapten antibodies have been investigated for a number of low-molecular weight targets.[8–14] These studies have revealed that hapten binding most often occurs at the interface between the heavy and light variable domains (i.e., VH and VL), where the two respective complementarity determining region 3 (CDR3) loops converge. Figure 1(A) displays an overlap of known anti-hapten antibody structures (which includes Fab and scFv fragments), illustrating the apparent canonical hapten binding site.

Interestingly, members of the *camelidae* family (e.g., camels and llamas) possess a subset of IgG antibodies lacking light chains, which results in antibodies possessing only a single variable domain, termed VHH,[15] that binds target molecules. These minimalist antibodies hold great potential as affinity reagents due to their small size, ease of recombinant production, and ideal biophysical properties.[16] Most importantly, despite their reduced binding interface, VHH (camelid) antibodies can possess affinities and specificities for their target protein molecules that rival conventional IgGs. Although the biophysical and structural mechanisms of VHH-protein interactions have been well characterized, detailed investigations into VHH-hapten interactions are lacking. For example, while several anti-hapten VHH antibodies have been produced against low-molecular weight molecules, such as a myotoxin,[17] caffeine,[18] picloram,[2] and reactive red dyes,[19,20] there is limited structural information revealing the detailed mechanisms of hapten recognition. Currently, only three hapten/VHH complexes have been published, two involve reactive red dye haptens[19,20] and another involves a small peptide.[21] Despite the absence of a VL domain, the hapten recognition mechanism of these VHH complexes closely mimics traditional VH/VL interfaces, where the hapten pocket is located at the former VL interface [Fig. 1(B)]. Nevertheless, the minimalist VHH architecture, lacking a defined binding pocket, would appear to be at a structural disadvantage when it comes to binding small molecule targets. Consequently, there are many unanswered questions regarding how high affinity and specificity may be achieved for VHH domains, which possess half the binding interface of conventional anti-hapten Fab/scFvs.

Here, we investigate the structure and binding thermodynamics of an anti-methotrexate (anti-MTX) VHH antibody. Unlike most anti-hapten camelid VHH antibodies, the anti-MTX VHH is reported to possess high affinity (low nanomolar K_d) for its MTX target.[22] To study the energetic and structural details of this unique camelid VHH, we produced the anti-MTX VHH through CDR grafting, where CDRs 1–3 published by Alvarez-Rueda *et al.*[22] were introduced into an existing anti-RNase A VHH framework. Structural data of existing hapten/VHH complexes, would suggest these three loops are sufficient for maintaining the necessary hapten/VHH contacts; however, the observed binding constant was 250-fold lower than the published value. The x-ray crystal structure of this MTX/anti-MTX CDR1-3 VHH graft revealed a previously unknown hapten binding site, located beneath CDR1. Interestingly, a nonhypervariable loop, "CDR4,"[23] which is in close proximity to CDRs1-3, is well posed for direct interactions with the MTX ligand. To test their potential role in MTX recognition, five residues from the original anti-MTX VHH CDR4 loop were introduced into the CDR1-3 graft, which resulted in a 1000-fold increase in affinity. The anti-MTX VHH CDR1-4 graft structure revealed the formation of several CDR4-mediated interactions as well as the structural basis for the observed high binding specificity for MTX over structurally similar ligands. Overall, these results suggest CDR1-based hapten recognition may provide a mechanism whereby heavy-chain only antibodies can compensate for the lack of a VH/VL interface. Furthermore, these results provide a cautionary case-study for CDR grafting, even when grafting is performed within the same family.

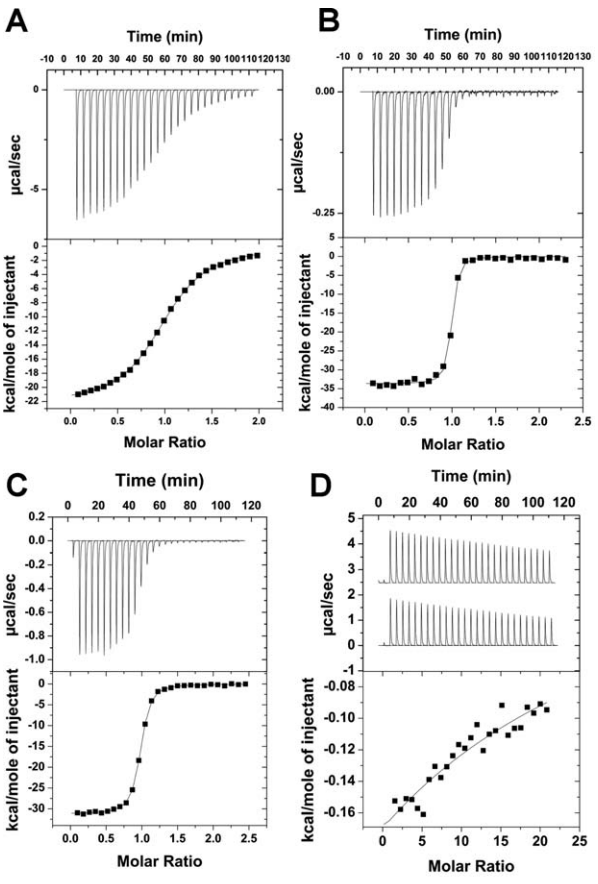

E

	CDR 4								
Residue #	74	75	76	77	78	79	80	81	82
CDR1-3 Graft	R	D	K	G	K	N	T	V	Y
CDR1-4 Graft	R	D	N	A	E	Y	L	V	Y

Figure 2. Representative ITC data for MTX binding anti-MTX VHH CDR1–3 (A) and CDR1–4 (B) VHH grafts. Representative ITC data for AMT (C) and FOL (D) binding anti-MTX VHH CDR1–4. All ITC data displayed were collected at 25°C. (E) Comparison of the CDR4 amino acid sequences between CDR1–3 and CDR1–4 grafts.

Results

Thermodynamic and structural characterization of the anti-MTX-VHH CDR1-3 graft complex

To explore the structure and energetic mechanisms of hapten/VHH interactions, a recently generated high affinity ($K_d = 29$ nM) anti-MTX VHH antibody[22] was produced. Based on the robust nature of VHH domains,[24,25] a graft-based method was pursued where the three hypervariable loops (CDRs 1–3) of the anti-MTX VHH antibody were introduced into the framework of an existing anti-RNase A VHH domain.[26,27] This graft-based approach was pursued for three main reasons. First, there is high level of sequence similarity between VHH frameworks. Second, we wished to exploit potential favorable crystal contacts afforded in the anti-RNase A VHH scaffold, which is well-suited for structural studies[26,27] and has crystallized in a variety of different space groups.[27,28] Third, available structural data of small ligand/VHH interactions, which includes two hapten/VHH complexes[19,20] and a peptide/VHH complex,[21] reveals a common target binding site that is located near the former VL interface (with respect to conventional VH/VL antibodies), where CDR3 and CDR2 loops make signficant intermolecular interactions with the target molecule [see Fig. 1(B)]. Consequently, a graft of CDRs1-3 would likely introduce the relevant interface residues.

Isothermal titration calorimetry (ITC) was used to investigate the thermodynamic basis for MTX/anti-MTX VHH CDR1-3 graft recognition. Representative ITC data for the 1:1 MTX/anti-MTX VHH graft binding event are presented in Figure 2(A) and the binding thermodynamics at 25°C are presented in Table I. The observed equilibrium dissociation constant, K_d, was 6.7 $\pm$ 0.9 μM, corresponding to a binding free energy change, ΔG°, of −7.1 $\pm$ 0.3 kcal/mol. The MTX/anti-MTX VHH CDR1-3 interaction

Table I. *Binding Thermodynamic for Methotrexate and the Two Anti-MTX VHH Grafts at 25°C*

	n	ΔH° (kcal/mol)	$-T\Delta S^\circ$ (kcal/mol)	ΔG° (kcal/mol)	ΔC_p (kcal/mol/K)	K_d (nM)
CDR1–3 Graft	1.02	−21.8 ± 0.1	14.7 ± 2.8	−7.1 ± 0.3	−0.24 ± 0.02	6700 ± 900
CDR1–4 Graft	0.96	−33.7 ± 0.2	22.3 ± 0.3	−11.4 ± 0.2	−0.29 ± 0.02	5 ± 2

displayed a very large, favorable enthalpy ($\Delta H^\circ = -21.8 \pm 0.1$ kcal/mol) overcoming an entropic penalty ($-T\Delta S^\circ = 14.7 \pm 2.8$ kcal/mol). Overall, while an enthalpically favored/entropically unfavored binding event is not uncommon with antibody interactions,[29] the most striking result was the observed binding constant, which was 250-times weaker than the published value ($K_d = 29$ nM).[22]

To investigate the structural basis of MTX recogntion and its relation to the observed binding energetics, we determined the crystal structure of the MTX/anti-MTX VHH CDR1-3 complex at 1.7 Å resolution (Table II). Contrary to previously known anti-hapten antibody structures, which include conventional VH/VL antibody frameworks (e.g., scFv and Fab) and single VHH domains, the anti-MTX VHH CDR1-3 complex structure reveals a noncanonical hapten binding site. Rather than use the CDR3 loop and the former light-chain interface surface to form a binding site, MTX is inserted into what may be best described as a binding "tunnel," which is formed beneath the CDR1 loop [Fig. 3(A,B)]. VHH residues V4, W34, M36, A100, and Y120 form a hydrophobic pocket for the central, hydrophobic portion of MTX, while the pteridine moiety of MTX completely passes under the CDR1 loop forming hydrogen bonds through N1, NA2, and NA4 atoms to the R74 side chain (CDR4), T80 main chain oxygen (CDR4), and C24 main chain oxygen (framework), respectively. CDR4 interactions also include N79 which participates in van der Waals interaction by "clamping down" on the pteridine group, and the side chain nitrogen of R74, which forms a water mediated H-bond with N8 of MTX's pteridine moiety. Additionally, the sides chains of R28, S30, R32 (all in CDR1), can potentially participate in hydrogen bond and/or salt-bridge interactions with MTX's terminal carboxylic acid groups; however, these carboxylic acid groups were used in the conjugation of MTX to BSA for the original immunization and generation of the anti-MTX VHH antibody.[22] Consequently, their role in MTX recognition is likely to be limited.

A nonhypervariable loop helps achieve high affinity binding

A notable feature of the anti-MTX binding site is the proximity of the nonhypervariable CDR4[23] (or "70s"[30]) loop which includes residues R74, N79, and T80. These residues participate in direct interactions with the pteridine moiety of MTX [Fig. 3(B)]. As

Table II. *Crystallographic Statistics*

	CDR1–3 Graft free	CDR1–3 Graft complex	CDR1–4 Graft free	CDR1–4 Graft complex
Data collection (highest resolution)				
Space group	$P6_122$	$P6_122$	$P2_1$	$P2_1$
a, b, c	101.1, 101.1, 156.9	103.1, 103.1, 157.1	39.4, 59.2, 131.4	43.7, 57.6, 131.1
α, β, γ	90, 90, 120	90, 90, 120	90, 92.2, 90	90, 90.3, 30
Resolution range	20–1.71 Å	20–1.70 Å	50–1.85 Å	20–2.11 Å
Number of reflections (all/unique)	564,921/91,151 (50,807/9,093)	573,729/52,887 (22,542/3,866)	182,778/50,771 (18,156/4,907)	127,485/37,495 (12,309/3,730)
I/σ (overall)	10.26 (2.9)	34.4 (2.3)	14.32 (2.3)	8.73 (3.3)
R_{merge}	0.132 (0.67)	0.067 (0.475)	0.068 (0.414)	0.076 (0.331)
Completeness (%)	99.8 (99.5)	96.5 (72)	95.3 (96.6)	98.7 (99.5)
Redundancy	6.2 (6.2)	10.8 (6.7)	3.6 (3.7)	3.4 (3.3)
Refinement				
R_{work}/R_{free}	18.54/21.48 (25.0/26.2)	18.02/19.97 (25.0/26.2)	19.30/23.90 (25.8/29.4)	23.56/29.27 (30.8/38.4)
Average residues/chain				
VHH	131	131	131	131
MTX	0	1	0	1
Water	97	112	52	16
RMSD				
Bond lengths (Å)	0.0178	0.0152	0.0152	0.0150
Bond angles (°)	1.55	1.45	1.58	1.57
Chiral volume	0.1234	0.1436	0.1311	0.1503
Ramachandran plot statistics				
Preferred number (%)	460 (97.66%)	233 (98.31%)	573 (98.12%)	553 (94.85%)
Additional allowed (%)	11 (2.34%)	4 (1.69%)	11 (1.88%)	27 (4.63%)
Outliers (%)	0	0	0	3 (0.51%)

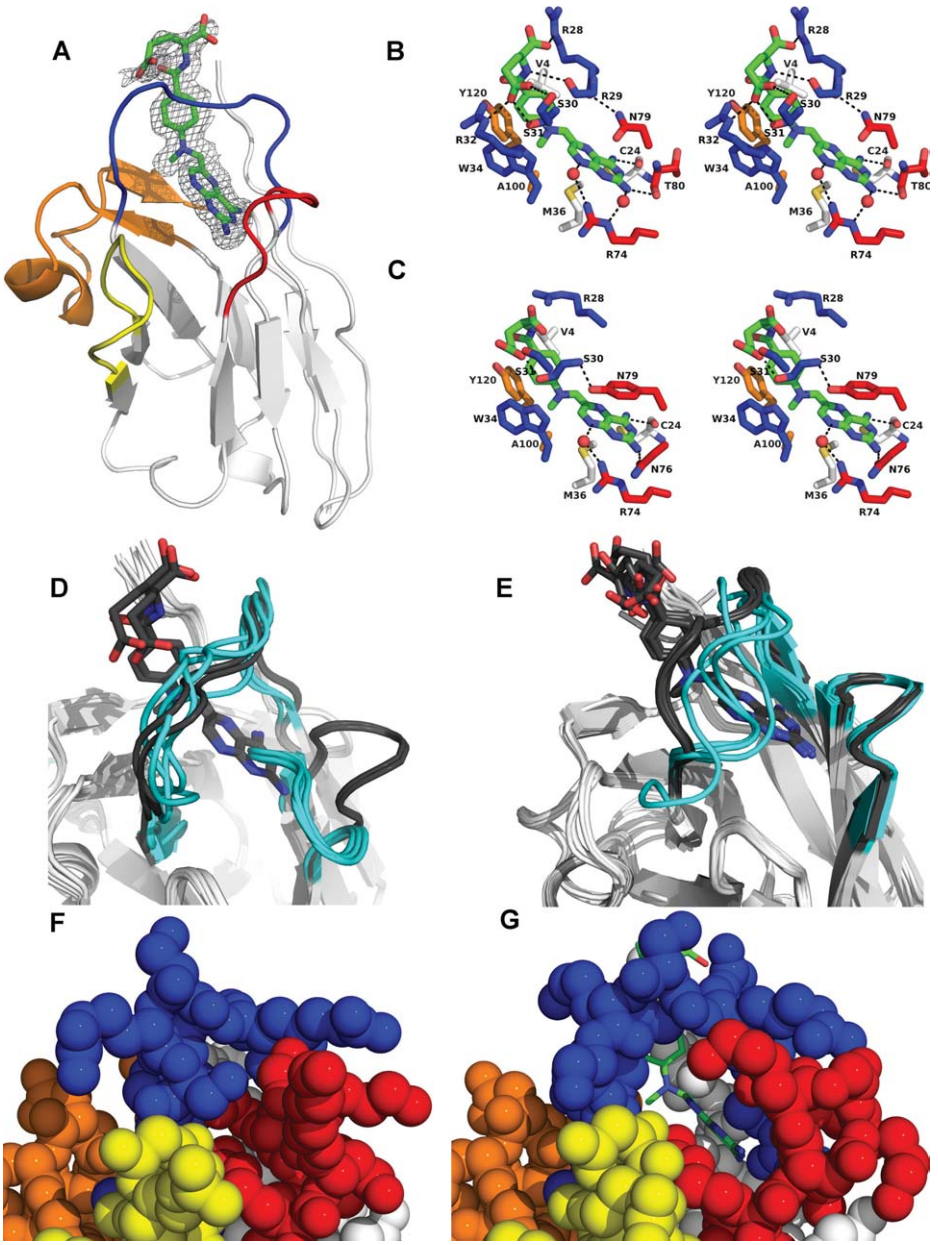

Figure 3. (A) Ribbon diagram of the MTX/anti-MTX VHH CDR1–3 graft complex with overlaid MTX omit difference map ($|F_o|$-$|F_c|$) contoured at 2σ. Stereo-view images of the MTX/anti-MTX VHH CDR1–3 (B) and MTX/anti-MTX VHH CDR1–4 (C) interfaces. CDR1 (blue), CDR2 (yellow), CDR3 (orange), CDR4 (red), framework (white), MTX (green), and waters (light red). Overlay of the free (cyan) and complex (dark grey) monomers in the asymmetric unit of the anti-MTX VHH CDR1–3 (D) and CDR1–4 (E) grafts. Space-filling models of the anti-VHH CDR 1–4 free (F) and complex (G) states [VHH orientation similar to that in panel (A) and color scheme identical to panels (A–C)].

there was no previous knowledge of nonhypervariable CDR4 loop residues participating (directly or indirectly) in hapten binding, the original anti-MTX CDR4 loop residues[22] were not introduced into the CDR1-3 VHH graft [Fig. 2(E)]. Consequently, this scenario opens an opportunity to determine the structural and energetic impact that proximal loops may play in hapten affinity and specificity. While the hydrogen bonding groups from main chain CDR4 residues are still present in both CDR4 sequences, the differences in CDR4 side chains could play a significant role in MTX recognition. To investigate the potential role these residues may play in MTX recognition, the five CDR4 residues from the original anti-MTX VHH[22] were introduced into the anti-MTX-VHH CDR1-3 graft to generate the anti-MTX VHH CDR 1-4-graft [Fig. 2(E)].

ITC was used to determine the thermodynamics for MTX/anti-MTX VHH CDR1-4 binding [Fig. 2(B)/Table I]. As with the CDR1-3 graft, a significant entropic penalty is observed which is overcome by a very favorable enthalpic contribution; however, both

are greater in magnitude than what was observed in the CDR1-3 graft binding thermodynamics. The resulting binding dissociation constant, K_d, is 5 ± 2 nM, which represents a 1000-fold higher binding affinity than the original CDR1-3 VHH graft ($\Delta\Delta G^\circ$ = −4.3 kcal/mol) and is in close agreement with the orignal published value (K_d = 29 nM).[22] The CDR1-3 and CDR1-4 grafts possessed change in heat capacity (ΔC_p) values of −240 ± 20 and −290 ± 20 cal/mol/K, respectively (Fig. 1, Supporting Information). The slightly more negative ΔC_p value for CDR1-4 VHH may suggest additional surface area is buried upon MTX binding.

To investigate the role of CDR4 in anti-MTX VHH CDR1–4's enhanced affinity, the crystal structure of the complex was determined to 2.1 Å resolution (Table II). Although there is no significant change in the interactions of MTX with CDR1, CDR3, and VHH framework residues as a result of the CDR4 graft, several changes are apparent within the newly grafted CDR4 loop [Fig. 3(C)]. Particularly, the water mediated hydrogen bond between the side chain Nε atom of R74 and the NA2 amine of the MTX's pteridine moiety is now replaced with a direct hydrogen bond with the side chain oxygen atom of N76. Additionally, Y79 replaces N79 above the pteridine moiety where its extends and buries additional hydrophobic surface and introduces potential π-stacking interactions. Y79 also forms a new hydrogen bond with the main chain NH group of S30 from CDR1, as opposed to the main chain oxygen of R28 that was hydrogen bonded to N79 within anti-MTX VHH CDR1-3. Finally, similar to the CDR1-3 graft, significant variability is observed between the terminal carboxylic acid moieties of the different MTX molecules in the asymmetric unit monomers. This functional group was used to conjugate MTX to BSA for immunization when generating the anti-MTX VHH antibody.[22]

Structural differences in the unbound anti-MTX grafts

As the overall binding energetics are determined by differences between the bound and the free states of anti-MTX VHH, the x-ray crystal structures of the free anti-MTX VHH CDR1–3 and CDR1–4 grafts were determined to 1.71 Å and 1.85 Å resolution, respectively (Table II). Contrary to the relatively minor structural differences that were observed in the two complex structures, more significant conformational changes are observed between the two unbound structures. Figure 3(D,E) present comparisons between the free and bound states for both CDR1-3 and CDR1–4 VHH grafts. The most notable difference is the CDR4 conformation within the CDR1–3 graft. Unlike the unbound CDR1–4 graft, where the CDR4 loop is observed in a conformation similar to the bound state, CDR1–3's CDR4 loop folds in toward the MTX binding site, which includes N79 partially filling the space occupied by MTX's pteridine group found in the complex structure. Based on N79's position in the free structure, it must move 4 Å (as defined by N79C_α) to accommodate insertion of the MTX ligand. Such a conformational change could likely include an energetic penalty toward MTX/CDR1-3 VHH binding, consistent with the observed binding constant.

Differences between the free and bound states are also observed with CDR1; however, potential connections to the observed binding energetics are not obvious. Superimposing the multiple VHH domains within their respective asymmetric unit reveals that the CDR1 loop samples several conformations in both CDR1–3 and CDR1–4 grafts. Notably, CDR1 of the CDR1–4 graft fills more of the MTX binding site [Fig. 3(E)]. This structural communication between the CDR1 and CDR4 loops is likely to play an intimate role in MTX recognition. According to our binding thermodynamic data, it appears that any potential negative consequences of the CDR1 loop variation in the CDR1-4 graft are overcome by the increased number of favorable CDR1-4 noncovalent interactions. Finally, it is important to note that these changes in CDR4 or CDR1 do not appear to be due to any direct crystal contact.

MTX/Anti-MTX VHH complexes bury significant surface area

An almost necessary requirement of the unique MTX binding pocket is the burial of significant surface area, as MTX inserts itself under and through the CDR1 loop [Fig. 3(A)]. The total change in solvent accessible surface area (VHH and MTX) upon MTX binding, ΔASA_{tot}, is 768 Å^{2}and 895 Å^2 for the CDR1-3 and CDR1-4 graft complexes, respectively. Notably, there is significant MTX surface burial in both complexes with 91% (576 Å^2) and 76% (480 Å^2) of the total accessible MTX surface area buried in the CDR1-4 and CDR1-3 complexes, respectively [Fig. 4(A–C)]. These values are quite striking when compared with conventional anti-hapten antibody complexes. To illustrate this feature, ΔASA calculations were performed on several anti-hapten antibody complexes, which possessed targets of comparable size to MTX (272–613 Da). Figure 5 displays the differences in hapten surface area burial for the two anti-MTX VHH grafts, an antireactive red dye/VHH complex, and nine representative conventional anti-hapten antibodies. Overall, the haptens in hapten/VHH complexes bury a larger amount of surface area versus haptens from their conventional antibody counterpart. These results are somewhat surprising considering the large interface present in conventional VH/VL antibodies (i.e., scFv and Fab

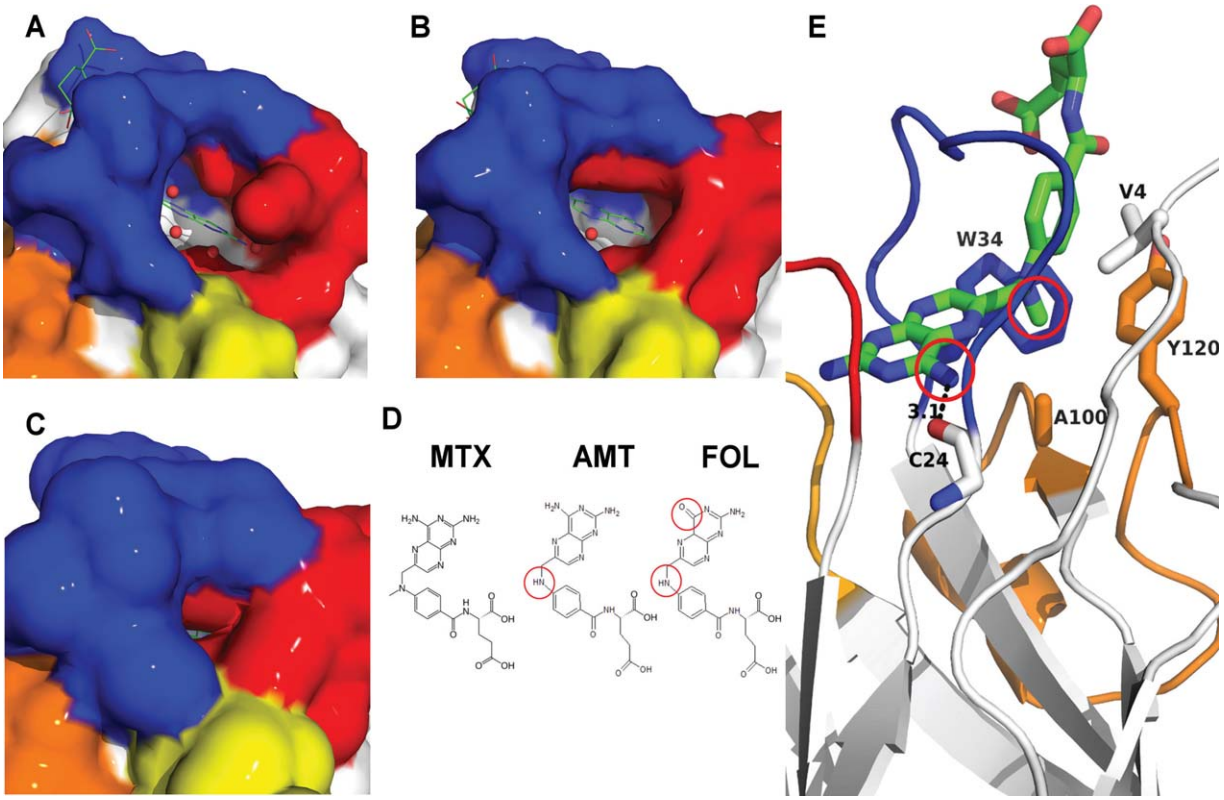

Figure 4. Molecular surface representation of the anti-MTX VHH CDR1-3 (A) and CDR1-4 (B) complexes. (C) Solvent accessible surface area representation of the anti-MTX VHH CDR1–4 complex. (D) Structure of MTX, AMT, and FOL. (E) Intermolecular contacts within the MTX/ VHH CDR1-4 complex structure that are related to MTX binding specificity. CDR1 (blue), CDR 3 (orange), CDR4 (red), framework (white).

complexes), where the hapten is typically "sandwiched" between both VH and VL domains.

Anti-MTX VHH specificity

Currently, there is limited data that reveals structure and energetic relationships for VHH-hapten specificity. The structural data of the two MTX/VHH complexes, as well as readily available MTX analogs, provides an opportunity to explore this issue of hapten/antibody specificity. Using ITC, we determined the binding thermodynamics for two related MTX analogs, aminopterin (AMT) and folate (FOL) [Table III/Fig. 4(D)]. When compared with MTX, AMT is missing the CM methyl group (located between the benzene and pteridine moieties), while FOL is missing the CM methyl group and substitutes a carbonyl oxygen for the NA4 amine in the pteridine group. Representative ITC data for the CDR1-4 graft binding AMT and FOL are shown in Figure 2(C,D), respectively.

Relative to MTX, the binding affinity toward AMT is moderately decreased, approximately 50-fold weaker for the CDR1-3 graft ($\Delta\Delta G^\circ = 2.3 + 0.2$ kcal/mol) and approximately 20-fold weaker for the CDR1-4 Graft ($\Delta\Delta G^\circ = 1.6 \pm 0.5$ kcal/mol). Figure 4(E) illustrates the predicted structural basis for the observed decrease in ligand affinity for AMT. The MTX/anti-MTX VHH complexes reveal the CM methyl group of MTX is buried in a hydrophobic

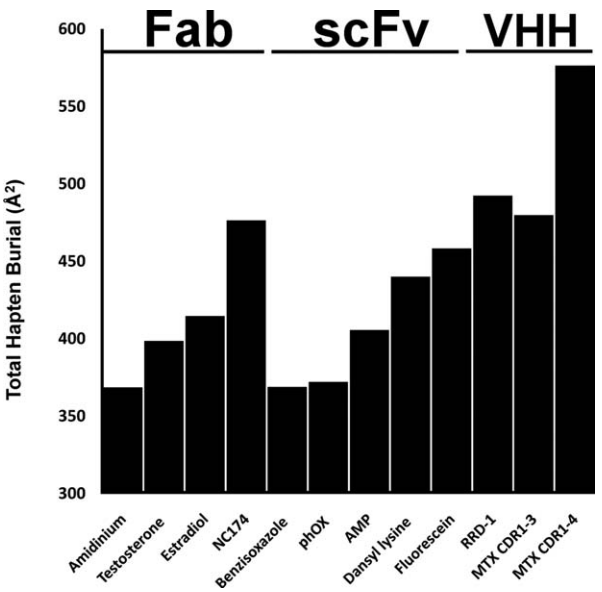

Figure 5. Total hapten buried surface area of representative anti-hapten antibodies (Fab, scFv, and VHH). PDB Codes: 1F3D, 1X9Q, 3KDM, 3FO0, 2CGR, 1WZ1, 2UUD, 1H8S, 1JNH, 1I3U.

Table III. *Anti-MTX VHH Binding Specificity Toward Related Ligands*

	n	ΔH° (kcal/mol)	$-T\Delta S^\circ$ (kcal/mol)	ΔG° (kcal/mol)	K_d	$\Delta\Delta G^\circ$ (kcal/mol)
anti-MTX-VHH CDR1–3 Graft						
MTX	1.02	−23 ± 1	16 ± 1	−7.14 ± 0.01	6 ± 1 μM	—
AMT	0.99	−21 ± 1	17± 1	−4.8 ± 0.1	290 ± 60 μM	2.3 ± 0.2
FOL	N/D	N/D	N/D	> −3.0	> 1 m*M*	N/D
anti-MTX-VHH CDR1–4 Graft						
MTX	0.96	−33.2 ± 0.3	21.7 ± 0.4	−11.4 ± 0.2	4 ± 1 nM	—
AMT	0.95	−33 ± 2	23 ± 2	−9.8 ± 0.4	80 ± 50 nM	1.6 ± 0.5
FOL[a]	1.0	−5 ± 1	0.9 ± 1	−4.1 ± 0.2	1.0 ± 0.2 m*M*	7.3 ± 0.3

[a] Experiments performed following methods of Turnbull and Daranas for low c-value titrations.[31]

binding pocket formed by residues V4, A100, W34, and Y120. Due to the absence of the CM methyl group in AMT, these favorable hydrophobic interactions would be reduced, thus providing a possible structural basis for reduced affinity. The relative differences in binding affinity between MTX and AMT (where the only difference is the loss of the CM methyl group) binding CDR1-3 and CDR1-4 (where the only difference is the CDR4 sequence) provide a thermodynamic cycle to probe the network of interactions across the interface. As the CDR1–4 VHH displays a smaller decrease in affinity relative to the CDR1–3 variant when binding AMT versus MTX, the calculated $\Delta\Delta\Delta G^\circ$ is -0.7 ± 0.5 kcal/mol. This small, but favorable value may suggest that the CDR4 loop, despite direct interaction with the CM group of MTX, may play an auxiliary role in stabilizing either the CDR1 loop or the hydrophobic binding pocket, which lead to enhanced interactions at the CM methyl group binding pocket.

While modest loss of affinity is observed with AMT, the binding affinity towards FOL is significantly decreased. In fact, no measurable binding is observed for the CDR1–3 graft (estimated as >1000-fold weaker than MTX binding), whereas the anti-MTX CDR1-4 graft possessed a $K_d = 1.0 \pm 0.2$ m*M* for binding FOL, which corresponds to a dramatic 10^5-fold decrease in binding constant relative to MTX ($\Delta\Delta G^\circ = 7.3 \pm 0.3$ kcal/mol). Consequently, the amine to carbonyl oxygen substitution at position NA4 in AMT, which is a reversal in hydrogen bonding properties, is likely critical to the discrimination between MTX and AMT, with an estimated energetic loss of ~6 kcal/mol, assuming strict additivity with the CM methyl group. The structures of both MTX complexes reveal that the main chain carbonyl oxygen of C25 participates as a hydrogen bond accepter for the NA4 amine within MTX, whereas FOL's carbonyl oxygen would appear to create significant energetic strain, as there is not a corresponding hydrogen bond donor in this region of the binding interface. Additionally, as the original hydrogen bond involves the main chain carbonyl of C25, which is a framework residue of VHH, there appears very little room for the antibody to accommodate the hydrogen bond mismatch through conformational change, thus suggesting a relatively rigid binding pocket. However, crystal structures of VHH complexes with AMT and FOL would ultimately be necessary to address whether any compensatory mechanisms exist.

Discussion

A common theme of heavy-chain only antibodies is "*doing more with less*." This is certainly the case for anti-hapten camelid VHH antibodies. As compared to conventional anti-hapten antibodies, which primarily use the VH/VL interface to recognize low-molecular weight ligands, VHH domains would apparently possess a disadvantage in their ability to recognize small molecule haptens. However, biophysical and structural data have revealed that camelid VHH domains can recognize haptens using multiple mechanisms, including using the former VH/VL interface,[19,20] as well as VHH homodimerization.[32] Here, structural and energetic studies of the anti-MTX VHH complex revealed a new hapten binding site, which allows significant MTX penetration and surface area burial. Interestingly, the amount of hapten surface burial exceeds the amount found in conventional VH/VL antibodies targeting low molecular weight ligands (< 700 Da). Ultimately, the increased interaction surface likely plays a key role in acquiring both high affinity and specificity toward the MTX target.

Through a somewhat fortuitous route, the non-hypervariable CDR4 loop was found to contribute greatly to high-affinity MTX recognition. While such contributions from neighboring scaffold residues are perhaps not overly surprising, as CDR4 has been used to affinity mature a conventional FAB antibody,[33] the magnitude of CDR4's contribution is significant (1000-fold effect on K_d). Additionally, while CDR4 loop conformations were similar between CDR1-3 and CDR1-4 grafts, structures of the unbound states revealed significant changes in CDR4 conformation. Particularly, a correlation in CDR4 and CDR1 conformations is observed in the unbound structures of the two different VHH grafts [compare unbound states in Fig. 3(D,E)], which likely contributes to the overall observed binding energetics. Extrapolating this finding to future

antibody engineering efforts, it is clear that assumptions of CDR loop participation in target recognition are likely to be nontrivial when based on amino acid sequence alone. While, future biophysical studies will be needed to dissect the role of CDR4's inter- and intra-molecular interactions, these findings have significant implications for VHH grafting and interface engineering techniques, such as the development of universal VHH scaffolds that possess desired biophysical properties (e.g., high thermal stability)[25] and synthetic, *in vitro* affinity maturation strategies.[27] Both approaches require defining interface versus noninterface residues when designing the graft or synthetic libraries. The anti-MTX VHH grafts provides a case-study demonstrating there can be a fine-line in defining contributing versus noncontributing residues. This is likely to be particularly true for VHH domains that bind low-molecular weight targets, where intermolecular contacts are concentrated to a smaller number of interface residues and can possess a significant energetic role in molecular recognition.

Overall, our results suggest heavy chain–only antibodies can be quite malleable in their recognition of low molecular weight targets. While only limited structural data exists for VHH/hapten complexes, questions remain concerning just how common the CDR1 binding "tunnel" might be. Similarly, it is not possible to say whether such a site would or would not be possible with conventional VH/VL antibodies. These observations are certainly interesting and may open unique opportunities to develop new anti-hapten VHH interactions through synthetic library approaches as well as raise awareness for potential pitfalls in antibody grafting and engineering. Ultimately, biophysical and structural studies on numerous structurally different hapten targets will be necessary to help distinguish fundamental differences in single (VHH) versus double (VH/VL) domain hapten binding sites.

Materials and Methods

Generation and production of the anti-MTX VHH

Using a pET-21a(+) vector (Novagen) containing the gene for an anti-RNase A VHH domain,[26,27] Kunkel Mutagenesis[34] was performed to replace CDR loops with that of an anti-MTX VHH (ID:3.4).[22] The following oligonucleotide sequences were used in generating CDR1-3 and CDR1-4 grafts:

CDR1(5′GTGCTTGACGGAACCAAGCCATAGCCC AGGAACGGGAGGAACGACGGGATGCTGCGCAGC TCAG3′),*CDR2(5′*GCCTTTCACGCTATCGCCATAG GTGGTCAGACGGCCATCGCCGCTAATTTTCGCC ACAAATTCACGTTCTTTGCCCGG),*CDR3(5′*GGTC ACATAGTTATCATCAGCAGCGCAGTAGTAAACTGC GGTGTCTTCTGG3′),*CDR4*(5′GCTGTCCATCTGCA GATACACCAGATATTCCGCGTTGTCACGGCTGAT GGTG3′) and *R114Q*(5′GGTTACTTGGGTGCCCTG GCCCCAATAATCCGG3′).

The sequence of the resulting CDR1-3 and CDR1-4 pET21a(+)-anti-MTX-VHH vectors, were verified by DNA sequencing. The primer for the mutation R114Q was designed to correct for an error in the CDR3 primer design. Overall, four framework residues, including Q6, P14, D89, and R116 were not included in the final anti-MTX VHH CDR1–4 graft. Based on the work described here, these are VHH scaffolding residues and greater than 10 Å from the binding interface. A sequence comparison between the original anti-RNase A VHH (cAb-RN05),[26] the anti-MTX VHH generated by Alvarez-Rueda *et al.*,[22] and the two grafts produced here (CDR1-3 and CDR1-4) is presented in Figure 2, Supporting Information.

Expression and purification

A 5 mL LB broth containing 100 μg/mL ampicillin was inoculated with a single colony of BL21(DE3) *E. coli* expression strain containing pET21a(+)-anti-MTX VHH. After overnight incubation at 37°C, a 50 mL LB/amp subculture was inoculated with 1 mL of the overnight culture. The subculture was subsequently used to inoculate a 1 L LB/amp culture. Expression of anti-MTX VHH was induced with 0.2 m*M* IPTG when the cells reached mid-log phase ($OD_{600} = 0.55$) and were incubated overnight at 20°C with shaking. Cells were harvested by centrifugation at 8000*g* for 15 min. The supernatant was decanted and the pellet was frozen (−20°C). The pellet was resuspended in 10 m*M* Tris/pH 8 and sonicated for 6, 30 s on/off cycles with a Model 60 Sonic Dismembrator (Fisher Scientific) at an output power of 21 Watts. The lysed cells were centrifuged at 22,700*g* for 15 min, and the supernatant was isolated. The soluble fraction was loaded on a Histrap HP column (GE Healthcare) and a 70 mL linear gradient of 20 m*M* to 500 m*M* imidazole (50 m*M* phosphate and 500 m*M* NaCl) was used to elute the His-tagged VHH protein. A single peak corresponding to the anti-MTX VHH was further purified on a HiLoad 26/60 Superdex 75 prep grade FPLC column (10 m*M* Tris, 150 m*M* NaCl, pH 8.0). The His-flag-Tev purification tag was removed using a 25:1 w/w ratio of VHH to TEV protease. The anti-MTX VHH was isolated by loading the TEV reaction solution on a Histrap HP column and collecting the flow-through and subjected to a final gel filtration column (Superdex 75 FPLC column).

Isothermal titration calorimetry

All ITC experiments were performed using a Microcal VP-ITC titration calorimeter (MicroCal, LLc, Northampton, MA) and performed over a range of temperatures from 15 to 35°C. All protein samples were dialyzed overnight against 4 L of PBS buffer

(20 m*M* sodium phosphate, 150 m*M* NaCl, pH 7.4) to ensure proper buffer matching. MTX (Sigma-Aldrich, St. Louis, MO) and AMT (MP Biomedicals, Solon, OH) were each dissolved in DMSO and then diluted into PBS buffer. DMSO was added to anti-MTX VHH solutions at a final 1% concentration to ensure matched buffers. FOL (Fisher Bioreagents, Pittsburg, PA) was dissolved directly into PBS buffer. MTX and FOL concentrations were determined using published (Merk Index) extinction coefficients, ε_{258nm} = 23,250 M^{-1} cm^{-1} and ε_{284nm} = 24,400 M^{-1} cm^{-1}, respectively. AMT concentration were determined ε_{284nm} = 24,400 M^{-1} cm^{-1}.[35] The concentrations of anti-MTX VHH CDR1–3 and CDR1–4 grafts were determined using extinction coefficients ε_{280nm} = 32,555 M^{-1} cm^{-1} and ε_{280nm} = 34,045 M^{-1} cm^{-1}, respectively, which were determined by the method of Pace *et al*.[36] Concentration values were measured in triplicate and the average value was used as the final concentration. CDR1-3 graft experiments were performed using between 1 m*M* and 9.5 m*M* ligand in the syringe and 0.085 m*M* to 0.1 m*M* to anti-MTX VHH in the cell. CDR4 graft experiments were performed at 30 μM to 3 m*M* ligand in the syringe and 3 μM to 300 μM anti-MTX VHH in the cell. Experiments with low "c" values (e.g., the low affinity FOL/anti-MTX VHH CDR1–4 complex) followed methods of Turnbull and Daranas.[31] Data analysis of these experiments included fixing the binding stoichiometry to 1.0. Generally, ITC experiments included a total of 28, 10 μL injections made every 200 s with a stirring speed of 307 rpm. Heats of dilution were accounted by subtracting the average of the postsaturation heats or the individual heats of dilution from a ligand dilution experiment. To account for dilution across the needle during equilibration, an initial 2 μL injection was discarded. Data were analyzed using Origin and the ITC add-on supplied by the manufacturer.

Crystallization of the anti-MTX VHH

The anti-MTX CDR1-3 and CDR1-4 VHH grafts were each run on a Superdex 75 model 10/30GL size exclusion column (GE Healthcare) with a 10 m*M* Tris, 300 m*M* NaCl, pH 8.0 running buffer. Fractions containing VHH were concentrated to 20 mg/mL using an Amicon ultrafiltration device with a 5-kDa cutoff membrane. Complex solutions were generated by adding a 4× and 1.5× concentration of MTX to the CDR1–3 and CDR1–4 graft, respectively. All crystals were grown by the hanging drop method. A total of 2 μL of 10 mg/mL free or complex CDR1-3 VHH graft were mixed with 2 μL of 3.5*M* NaFormate, pH 7.0 or 1.0*M* Succinic acid, 0.1*M* HEPES, 1% w/v PEG monomethyl ether 2000, pH 7.0, respectively. Clear hexagonal crystals began to appear after two days. 2 μL of 20 mg/mL free or complex CDR1-4 VHH were mixed with 2 μL of 0.2*M* lithium sulfate, 0.1*M* BIS-TRIS pH 6.5, 25% PEG 3,350, or 2 μL 0.2*M* lithium sulfate monohydrate, 0.1*M* Tris pH 8.5, 25% PEG 3350, respectively. Clear, rectangular crystals appeared after four days for the free and complex CDR1–4 VHH. 20% glycerol or MPD was used as a cryoprotectant. All x-ray data sets were collected at the Advanced Photon Source at Argonne National Laboratories, Argonne, Illinois The CDR1-3 VHH complex data were collected at the LS-CAT-21ID-G beamline (0.979 Å), all other data sets were collected at the SER-CAT-22BM beam-line at (1 Å).

X-ray structure solution

Data were indexed, merged, and scaled using HKL-2000.[37] Molecular replacement was performed using Phaser[38] with an existing anti-Reactive Red Dye VHH (PDB ID:1I3U) as the search molecule. For the CDR1–3 graft complex 2 molecules were found in the asymmetric unit (ASU). For the free CDR1–3 graft 4 molecules were found in the ASU. Both the free and complex CDR4 graft structures possessed five molecules in the ASU. The CCP4 (Refmac) program suite was used for all refinement.[39] The CDR residues were removed during the initial refinement and were subsequently re-built using iterative rounds of refinement and model building using Coot.[40] Density corresponding to the MTX was clearly visible in the complex structures after two rounds of refinement in Refmac. The final structure of the free CDR1–4 VHH structure does not possess residues 28–32 in chain C as they are not resolved in the electron density. The CDR1–4 VHH/MTX bound structure is well resolved for 4 of the 5 chains in the ASU. Other than in close proximity to the MTX binding site, chain E was not as well resolved. To improve the poor refinement statistics associated with Chain E, medium NCS restraints were added for chain E against the average of chains A–D for CDR1–4 models. Also, the terminal carboxylic acid groups of the MTX in chain C and residues 125–128 in chain E were not included as they were not well resolved in the electron density. Finally, the terminal carboxylic acid groups of the MTX in chain C were not included as they were not resolved. All structures have been deposited in the PDB, including, anti-MTX CDR1–3 free (ID: 3QXU), MTX/CDR1–3 complex (ID: 3QXT), CDR1–4 free (ID: 3QXW), and MTX/CDR1–4 (ID: 3QXV). All molecular images were generated using PYMOL.[41] Accessible Surface Area calculations were calculated using the program NACCESS.[42]

Acknowledgments

The authors thank Dr. R. Walters for assistance with x-ray data collection and helpful discussions. They also thank C. Smith and M. Murtaugh for reading the article. Use of the Advanced Photon Source was supported by the U. S. Department of Energy, Office of Science, Office of Basic Energy Sciences, under Contract No. W-31-109-

Eng-38. Use of the LS-CAT Sector 21 was supported by the Michigan Economic Development Corporation and the Michigan Technology Tri-Corridor for the support of this research program (Grant 085P1000817). Data were also collected at Southeast Regional Collaborative Access Team (SER-CAT) 22-BM beamline, Argonne National Laboratory. Supporting institutions may be found at www.ser-cat.org/members.html.

References

1. Zhang H, Zhang Y, Wang S (2008) Development of flow-through and dip-stick immunoassays for screening of sulfonamide residues. J Immunol Methods 337:1–6.
2. Yau KYF, Groves MAT, Li SH, Sheedy C, Lee H, Tanha J, MacKenzie CR, Jermutus L, Hall JC (2003) Selection of hapten-specific single-domain antibodies from a non-immunized llama ribosome display library. J Immunol Methods 281:161–175.
3. Song SS, Lin F, Liu LQ, Kuang H, Wang LB, Xu CL (2010) Immunoaffinity removal and immunoassay for rhodamine B in chilli powder. Int J Food Sci Tech 45:2589–2595.
4. Hofstetter O, Lindstrom H, Hofstetter H (2002) Direct resolution of enantiomers in high-performance immunoaffinity chromatography under isocratic conditions. Anal Chem 74:2119–2125.
5. Curd J, Smith TW, Jaton JC, Haber E (1971) Isolation of digoxin-specific antibody and its uses in reversing effects of digoxin. Proc Natl Acad Sci USA 68:2401.
6. Smith TW, Butler VP, Haber E, Fozzard H, Marcus FI, Bremner WF, Schulman IC, Phillips A (1982) Treatment of life-threatening digitalis intoxication with digoxin-specific Fab antibody fragments—experience in 26 cases. New Engl J Med 307:1357–1362.
7. Fox BS, Kantak KM, Edwards MA, Black KM, Bollinger BK, Botka AJ, French TL, Thompson TL, Schad VC, Greenstein JL, Gefter ML, Exley MA, Swain PA, Briner TJ (1996) Efficacy of a therapeutic cocaine vaccine in rodent models. Nat Med 2:1129–1132.
8. Monnet C, Bettsworth F, Stura EA, Le Du MH, Menez R, Derrien L, Zinn-Justin S, Gilquin B, Sibai G, Battail-Poirot N, Jolivet M, Menez A, Arnaud M, Ducancel F, Charbonnier JB (2002) Highly specific anti-estradiol antibodies: structural characterisation and binding diversity. J Mol Biol 315:699–712.
9. Burmester J, Spinelli S, Pugliese L, Krebber A, Honegger A, Jung S, Schimmele B, Cambillau C, Pluckthun A (2001) Selection, characterization and x-ray structure of anti-ampicillin single-chain Fv fragments from phage-displayed murine antibody libraries. J Mol Biol 309:671–685.
10. Scotti C, Gherardi E (2006) Structural basis of affinity maturation of the TEPC15/Vkappa45.1 anti-2-phenyl-5-oxazolone antibodies. J Mol Biol 359:1161–1169.
11. Nakasako M, Oka T, Mashumo M, Takahashi H, Shimada I, Yamaguchi Y, Kato K, Arata Y (2005) Conformational dynamics of complementarity-determining region H3 of an anti-dansyl Fv fragment in the presence of its hapten. J Mol Biol 351:627–640.
12. Guddat LW, Shan L, Anchin JM, Linthicum DS, Edmundson AB (1994) Local and transmitted conformational changes on complexation of an anti-sweetener Fab. J Mol Biol 236:247–274.
13. Niemi MH, Takkinen K, Amundsen LK, Soderlund H, Rouvinen J, Hoyhtya M (2011) The testosterone binding mechanism of an antibody derived from a naive human scFv library. J Mol Recogn 24:209–219.
14. Midelfort KS, Hernandez HH, Lippow SM, Tidor B, Drennan CL, Wittrup KD (2004) Substantial energetic improvement with minimal structural perturbation in a high affinity mutant antibody. J Mol Biol 343:685–701.
15. Hamers-Casterman C, Atarhouch T, Muyldermans S, Robinson G, Hamers C, Songa EB, Bendahman N, Hamers R (1993) Naturally occurring antibodies devoid of light chains. Nature 363:446–448.
16. Muyldermans S (2001) Single domain camel antibodies: current status. J Biotechnol 74:277–302.
17. Doyle PJ, Arbabi-Ghahroudi M, Gaudette N, Furzer G, Savard ME, Gleddie S, McLean MD, Mackenzie CR, Hall JC (2008) Cloning, expression, and characterization of a single-domain antibody fragment with affinity for 15-acetyl-deoxynivalenol. Mol Immunol 45:3703–3713.
18. Ladenson RC, Crimmins DL, Landt Y, Ladenson JH (2006) Isolation and characterization of a thermally stable recombinant anti-caffeine heavy-chain antibody fragment. Anal Chem 78:4501–4508.
19. Spinelli S, Frenken LGJ, Hermans P, Verrips T, Brown K, Tegoni M, Cambillau C (2000) Camelid heavy-chain variable domains provide efficient combining sites to haptens. Biochemistry 39:1217–1222.
20. Spinelli S, Tegoni M, Frenken L, van Vliet C, Cambillau C (2001) Lateral recognition of a dye hapten by a llama VHH domain. J Mol Biol 311:123–129.
21. De Genst EJ, Guilliams T, Wellens J, O'Day EM, Waudby CA, Meehan S, Dumoulin M, Hsu ST, Cremades N, Verschueren KH, Pardon E, Wyns L, Steyaert J, Christodoulou J, Dobson CM (2010) Structure and properties of a complex of alpha-synuclein and a single-domain camelid antibody. J Mol Biol 402: 326–343.
22. Alvarez-Rueda N, Behar G, Ferre V, Pugniere M, Roquet F, Gastinel L, Jacquot C, Aubry J, Baty D, Barbet J, Birkle S (2007) Generation of llama single-domain antibodies against methotrexate, a prototypical hapten. Mol Immunol 44:1680–1690.
23. Bond CJ, Wiesmann C, Marsters JC, Jr, Sidhu SS (2005) A structure-based database of antibody variable domain diversity. J Mol Biol 348:699–709.
24. Ewert S, Honegger A, Pluckthun A (2004) Stability improvement of antibodies for extracellular and intracellular applications: CDR grafting to stable frameworks and structure-based framework engineering. Methods 34:184–199.
25. Saerens D, Pellis M, Loris R, Pardon E, Dumoulin M, Matagne A, Wyns L, Muyldermans S, Conrath K (2005) Identification of a universal VHH framework to graft non-canonical antigen-binding loops of camel single-domain antibodies. J Mol Biol 352:597–607.
26. Decanniere K, Desmyter A, Lauwereys M, Ghahroudi MA, Muyldermans S, Wyns L (1999) A single-domain antibody fragment in complex with RNase A: non-canonical loop structures and nanomolar affinity using two CDR loops. Structure 7:361–370.
27. Koide A, Tereshko V, Uysal S, Margalef K, Kossiakoff AA, Koide S (2007) Exploring the capacity of minimalist protein interfaces: interface energetics and affinity maturation to picomolar K(D) of a single-domain antibody with a flat paratope. J Mol Biol 373:941–953.
28. Tereshko V, Uysal S, Koide A, Margalef K, Koide S, Kossiakoff AA (2008) Toward chaperone-assisted crystallography: protein engineering enhancement of crystal packing and X-ray phasing capabilities of a camelid single-domain antibody (VHH) scaffold. Protein Sci 17: 1175–1187.

29. Stites WE (1997) Protein-protein interactions: interface structure, binding, thermodynamics, and mutational analysis. Chem Rev 97:1233–1250.
30. Franklin MC, Carey KD, Vajdos FF, Leahy DJ, de Vos AM, Sliwkowski MX (2004) Insights into ErbB signaling from the structure of the ErbB2-pertuzumab complex. Cancer Cell 5:317–328.
31. Turnbull WB, Daranas AH (2003) On the value of c: can low affinity systems be studied by isothermal titration calorimetry? J Am Chem Soc 125:14859–14866.
32. Sonneson GJ, Horn JR (2009) Hapten-induced dimerization of a single-domain VHH camelid antibody. Biochemistry 48:6693–6695.
33. Baca M, Presta LG, O'Connor SJ, Wells JA (1997) Antibody humanization using monovalent phage display. J Biol Chem 272:10678–10684.
34. Kunkel TA (1985) Rapid and efficient site-specific mutagenesis without phenotypic selection. Proc Natl Acad Sci USA 82:488–492.
35. Mandelbaum-Shavit F, Grossowicz N (1973) Carrier-mediated transport of folate in a mutant of Pediococcus cerevisiae. J Bacteriol 114:485–490.
36. Pace CN, Vajdos F, Fee L, Grimsley G, Gray T (1995) How to measure and predict the molar absorption coefficient of a protein. Protein Sci 4:2411–2423.
37. Otwinowski Z, Minor W (1997) Processing of X-ray diffraction data collected in oscillation mode. Methods Enzymol 276:307–326.
38. McCoy AJ, Grosse-Kunstleve RW, Adams PD, Winn MD, Storoni LC, Read RJ (2007) Phaser crystallographic software. J Appl Cryst 40:658–674.
39. Collaborative Computational Project No. 4 (1994) The CCP4 suite: programs for protein crystallography. Acta Cryst D50:760–763.
40. Emsley P, Cowtan K (2004) Coot: model-building tools for molecular graphics. Acta Cryst D60:2126–2132.
41. DeLano WL (2002) The PyMOL Molecular Graphics System. San Carlos, CA, USA: DeLano Scientific.
42. Hubbard SJ, Thornton JM (1993) "NACCESS," Computer Program. Department of Biochemistry and Molecular Biology, University College London.